# Spectrally Engineering Photonic Entanglement with a Time Lens

J. M. Donohue,[1,*] M. Mastrovich,[1,2] and K. J. Resch[1,†]
[1]Institute for Quantum Computing and Department of Physics and Astronomy, University of Waterloo, Waterloo, Ontario, Canada N2L 3G1
[2]Department of Physics, Harvey Mudd College, Claremont, California 91711, USA
(Received 19 July 2016; published 6 December 2016)

A time lens, which can be used to reshape the spectral and temporal properties of light, requires the ultrafast manipulation of optical signals and presents a significant challenge for single-photon application. In this work, we construct a time lens based on dispersion and sum-frequency generation to spectrally engineer single photons from an entangled pair. The strong frequency anticorrelations between photons produced from spontaneous parametric down-conversion are converted to positive correlations after the time lens, consistent with a negative-magnification system. The temporal imaging of single photons enables new techniques for time-frequency quantum state engineering.

DOI: 10.1103/PhysRevLett.117.243602

Sources of single photons with precisely controlled properties are necessary for effective and efficient photonic quantum communication, computation, and metrology. The spectral, or energy-time, degree of freedom is of particular interest, as it can be used to encode information in a high-dimensional Hilbert space [1] and is naturally robust when transmitting through both long-distance fiber links [2] and photonic waveguides [3]. Entanglement in this degree of freedom is essential for applications such as high-dimensional quantum key distribution [1], nonlocal dispersion cancellation [4], and quantum-enhanced clock synchronization [5]. The nonlinear process of spontaneous parametric down-conversion (SPDC), for example, provides a reliable source of energy-time-entangled photons. Because of energy conservation, most SPDC sources tend to produce photons with frequency anticorrelations. However, photon pairs with positively correlated spectra may be useful for dispersion cancellation in long-distance channels [6] and quantum-enhanced clock synchronization [5]. Using SPDC sources with extended phase-matching conditions, joint spectra with positive spectral correlations have been produced before [6–9], but control over the correlations after state generation has not yet been demonstrated.

With linear optics, it is possible to shape the spectrum of single photons through frequency-dependent attenuation and phase shifts, as can be accomplished with pulse shapers and spatial-light modulators [10]. More complex transformations demand techniques such as those based on fast electro-optic devices or nonlinear optical processes. These are required for many quantum applications, such as interfacing with quantum memories [11], ultrafast photon switching [12], manipulating time-bin qubits [13–15], and temporal mode selection [3,16]. Spectral control over a photon after it has been created is therefore highly desirable for ultrafast manipulation and state engineering, especially at wavelengths where materials with suitable phase matching do not exist. Entanglement cannot be increased or decreased through a local unitary process. As a result, pulse shaping cannot be used to convert energy-time entangled states to uncorrelated states [17]. It can, however, be used to change the specific energy relations between the two photons or convert the correlation between the photon frequencies to a correlation between the frequency of one and the time of arrival of the other.

In this work, we demonstrate the ultrafast control of quantum-optical waveforms with subpicosecond features. We construct a temporal imaging system based on ultrafast nonlinear effects to manipulate the spectral profile of single photons. We apply this technique to half of an energy-time-entangled pair produced with SPDC and observe that the frequency anticorrelations are converted to positive correlations after the time lens through joint spectral intensity measurements, in addition to an adjustable central frequency shift. It is straightforward to adjust the temporal spectral magnification by changing the chirp parameters, and our scheme is free of intense broadband noise such as Raman scattering. A similar, as-yet-unrealized application of time lenses was proposed using electro-optic modulators [18].

Temporal imaging can be understood in direct analogy with its spatial counterpart [19,20]. It is instructive to compare the corresponding elements in each, as shown in Fig. 1. In spatial imaging, free-space propagation causes the momentum components to diverge in space, resulting in a spatial spread of the beam. The action of the lens is to shift the transverse momenta in a spatially dependent way, such that after further propagation the beam may refocus. Analogously, in temporal imaging, propagation through a dispersive material (such as an optical fiber) causes the constituent frequencies of a pulse to diverge in time, resulting in a temporal spread of the pulse. Constructing

 

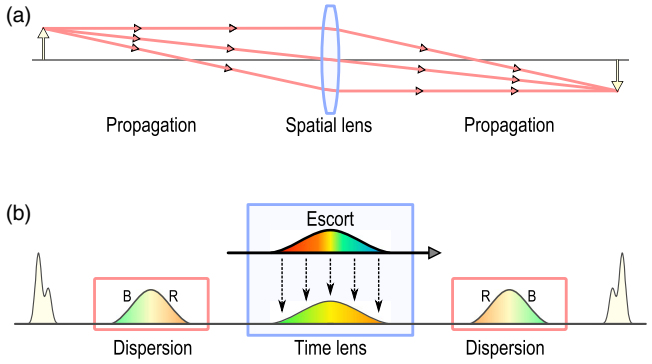


FIG. 1. Temporal shaping with an up-conversion time lens. (a) In a spatial imaging system, free-space propagation spreads the spatial extent of the beam such that each portion of the beam has a distinct transverse momentum, visualized with arrows. The lens shifts the momenta in a spatially dependent fashion, which effectively reverses the momenta for off-center components, and the beam refocuses with further spatial propagation. (b) The temporal imaging system operates through an analogous principle, where chromatic dispersion spreads the temporal profile of the beam such that each temporal slice of the beam has a distinct central frequency, ranging from a redshifted leading edge $R$ to a blueshifted tail $B$. The time lens introduces a time-dependent frequency shift, which can reverse the frequency shifts and allow the wave packet to refocus itself after more chromatic dispersion is applied. The temporal structure of the pulse will be reversed, akin to an imaging system with negative magnification. In our realization, we use sum-frequency generation with a dispersed escort pulse to implement an up-conversion time lens. At each time in the interaction, the signal interacts with a different frequency of the escort, effectively enforcing a time-dependent relative frequency shift as well as a change in the carrier frequency.

the equivalent of a lens for temporal imaging requires a time-dependent frequency shift in the same way that a spatial lens requires a spatially dependent transverse momentum shift. Self-phase modulation can approximate the required effect [20] but is ineffective for single-photon signals. Four-wave mixing has been shown to be effective for classical signals [21–26], but suppression of broadband noise sources presents a challenge for quantum signals. Recent work has shown great promise using cross-phase modulation in a photonic crystal fiber [27], Raman memories [28], and electro-optic modulators [29,30] to shape broadband single-photon waveforms.

The up-conversion time lens [31], seen in Fig. 1(b), is based on sum-frequency generation (SFG), a type of three-wave mixing in which two pulses may combine to produce a pulse at the sum of their frequencies. In the case of interest, one pulse is considered to contain a single photon and the other to be a strong classical pulse. This strong classical pulse, referred to as the *escort*, up-converts the photon to a new frequency, leaving its own imprint on the spectral shape of the up-converted photon. SFG has been shown to be a powerful and potentially efficient tool for ultrafast waveform manipulation which remains effective at the single-photon level [2,32–36]. The combination of SFG and pulse shaping enables the manipulation of ultrafast single-photon waveforms for techniques such as bandwidth compression [37], quantum pulse gates [16], and time-to-frequency conversion [14,23].

We represent the spectral field of a dispersed optical pulse as $F(\omega)e^{i\phi(\omega)}$, where the spectral phase has a quadratic frequency dependence $\phi(\omega) = A(\omega - \omega_0)^2$, with chirp parameter $A$. We characterize the dispersion applied to the input signal, escort pulse, and output waveform by the chirp parameters $A_i$, $A_e$, and $A_o$, respectively, which in the case of normal dispersion are proportional to the length of material passed through. We assume that the pulses are all chirped to many times their initial widths, known as the large-chirp limit. In this limit, the imaging equation for the time lens system shown in Fig. 1(b) can be found in Refs. [31,35] and simplifies to the relation [20,35]

$$\frac{1}{A_i} + \frac{1}{A_o} = -\frac{1}{A_e}. \tag{1}$$

This equation has the same form as the thin lens equation, with dispersion playing the role of the propagation distance and the escort chirp the role of the focal length.

In analogy to spatial imaging, the output waveform will have the same features as the input but scaled by a magnification factor [20,31,35]

$$M_{\text{spectral}} = \frac{1}{M_{\text{temporal}}} = \left(-\frac{A_i}{A_o}\right) = 1 + \frac{A_i}{A_e}. \tag{2}$$

The inverse relationship of the spectral and temporal magnification is a consequence of the scaling property of the Fourier transform. Because of this relationship, spectral measurements can be used to observe the time lens effect.

If $A_i = -2A_e$, the effective temporal and spectral magnification is $-1$, and both the temporal and spectral shapes will be reversed. If the input signal is a single photon which is spectrally entangled with a partner, reversing the spectrum of the photon will result in an overall reversal of the two-photon joint spectrum. The reversal of the spectral profile occurs as the photonic signal is chirped twice as strongly as the escort, such that every portion of the signal spectrum detuned from the central frequency by $\delta\omega$ meets a segment of the escort pulse detuned by $-2\delta\omega$ from its central frequency. In the large-chirp limit, only an output chirp $A_o$ is required to recompress the joint spectral state temporally, which has no effect on the spectral profile of the output but determines the output joint temporal distribution. A derivation may be found in Supplemental Material [38], Sec. I.

Our experimental setup is shown in Fig. 2 and is detailed in Supplemental Material [38], Sec. II. We create a signal

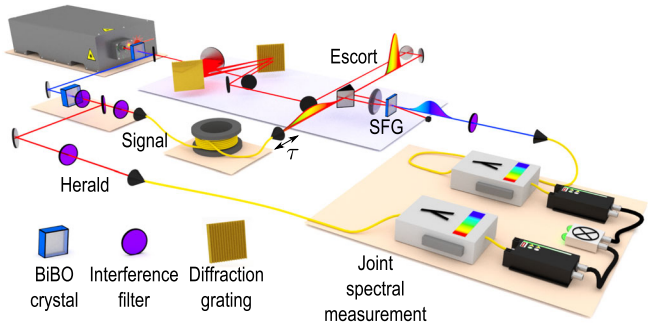


FIG. 2. Experimental setup. Frequency-entangled photons are created through the spontaneous parametric down-conversion of ultrafast pulses from a frequency-doubled Ti:sapphire laser. The signal photons are chirped through 34 m of single-mode fiber, while the remaining Ti:sapphire light comprises the escort pulse and antichirped in a grating-based pulse compressor. The pulses are recombined with relative delay $\tau$ for noncollinear sum-frequency generation (SFG). The up-converted signal is then isolated with bandpass filters and spectrally resolved in coincidence with the herald.

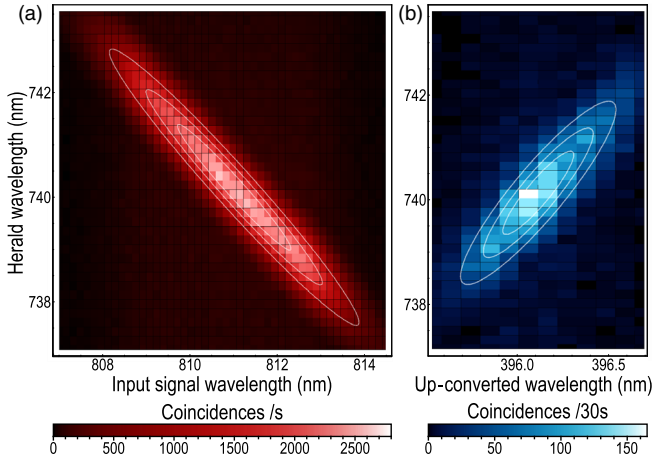


FIG. 3. Joint spectra. (a) The joint spectrum measured between the signal photon and the herald immediately after down-conversion has strong frequency anticorrelations, exhibiting a statistical correlation of $-0.9702 \pm 0.0002$ ($-0.9776 \pm 0.0009$ when corrected for finite spectrometer resolution). (b) After sum-frequency generation, the joint spectrum between the up-converted signal photon and the herald exhibits strong positive frequency correlations, with a statistical correlation of $+0.863 \pm 0.004$ ($+0.909 \pm 0.005$ resolution corrected). The white lines on each plot correspond to 25% contours of the resolution-corrected Gaussian fits. Background subtraction has not been employed in either image.

and herald photons through SPDC in 3 mm of bismuth borate (BiBO) stimulated by a pulsed laser. The down-converted photons are spectrally filtered and coupled into a single-mode (SM) fiber, from which they can each be sent to independent grating-based scanning spectrometers for spectral analysis, as seen in the initial joint spectrum in Fig. 3(a). The signal photons can be instead sent through 34 m of SM fiber, where they are positively chirped by normal dispersion. The escort laser pulse passes through a grating-based compressor, set to apply half the dispersion as the fiber with the opposite sign [37]. The escort and signal photon are combined for SFG in 1 mm of BiBO, and the up-converted photon is measured with another scanning spectrometer in coincidence with the herald. The combined efficiency of the chirp, up-conversion, and fiber coupling is approximately 0.2%. Detection events from the herald spectrometer were measured in coincidence with the up-converted photon spectrum, and the measured joint spectrum is shown in Fig. 3(b).

The output joint spectrum exhibits clear positive frequency correlations, in contrast with the clear anticorrelations seen in the input joint spectrum. The measured joint spectra were then fit to a two-dimensional Gaussian. All spectrometers used had a spectral resolution of approximately 0.1 nm. While this resolution allowed us to resolve the essential spectral features, this finite resolution is on the same order of magnitude as our spectral bandwidths, which broadened their measured features. To account for the limited resolution, we deconvolved the fit spectra with a Gaussian spectrometer response function. The fit parameters of the joint spectra produced from our SPDC source and after SFG are shown in Table I. The statistical correlation of the signal and herald wavelengths $\rho$, defined as the covariance of two parameters divided by the standard deviation of each, is statistically significant both before and after the time lens. The negative-to-positive change of $\rho$ indicates the reversal of the correlations.

Assuming that the two-photon state is pure and coherent, we have succeeded in manipulating energy-time entanglement. Previous experiments have established that photons created through SPDC are energy-time entangled rather than classically correlated [39] and that SFG maintains coherence [2,14,36]. Modeling our experiment under these

TABLE I. Joint spectral state parameters. Selected properties of the Gaussian fits to the joint spectra seen in Fig. 3 are given. The values are all corrected for the finite resolution of the spectrometers, and the widths are full width at half maximum. The bandwidth of the herald photon is reduced when measured in coincidence with the up-converted signal due to the finite temporal width of the chirped escort and the frequency correlations in the initial joint spectrum. The correlation parameters show that the spectral correlation is present after the time lens but has changed from anticorrelation to positive correlation. The second-order cross-correlation $g^{(2)}_{s,h}$ is significantly greater than 2, indicating nonclassical statistics.

| Property | Input | Output |
|---|---|---|
| Signal bandwidth | $(1.840 \pm 0.003)$ THz | $(1.14 \pm 0.02)$ THz |
| Herald bandwidth | $(2.034 \pm 0.003)$ THz | $(1.35 \pm 0.02)$ THz |
| Correlation $\rho$ | $-0.9776 \pm 0.0009$ | $0.909 \pm 0.005$ |
| $g^{(2)}_{s,h}$ | $4.190 \pm 0.002$ | $3.34 \pm 0.03$ |

assumptions, our data show that the photon pairs have been converted from energy-time-entangled states with strong frequency anticorrelations to ones with strong frequency correlations. The temporal distribution is not uniquely specified by the joint spectrum, as the spectral phase remains unknown. However, if the state is indeed pure, the spectral phase could be compensated to make a transform-limited distribution with tight temporal anticorrelations. To directly measure the time-domain distribution requires a time resolution on the order of femtoseconds, which is much shorter than the resolution of our photon counters. The time scale of our experiment could be measurable with additional nonlinear processes [7], and energy-time entanglement could be directly confirmed through a nonlocal interference experiment with additional temporal selection [40].

We also calculate the second-order cross-correlation function between the signal and herald photon $g^{(2)}_{s,h} = (P_{s\&h}/P_s P_h)$ when the two photons are coincident in time, where $P_i$ is the probability of measuring a photon in mode $i$, by comparing the coincidences with the single-detection events before the spectrometers [11,28]. A value larger than two indicates nonclassicality if we assume that the individual second-order statistics of the signal and herald are at most thermal (as expected for a single-photon state) [28]. The values of the second-order cross-correlation function of the herald with the initial and up-converted signal photon are given in Table I and are significantly larger than two in both cases. The lower $g^{(2)}_{s,h}$ value of the up-converted light can be attributed to the spectrally distinguishable uncorrelated second-harmonic background which reaches the detectors. An extensive list of measured parameters, including other correlation quantifiers, may be found in Supplemental Material [38], Sec. II.

While the up-conversion efficiency of the time lens in our experiment is low, the limitations are practical rather than fundamental [35]. As the escort used in our experiment is approximately the same spectral width as the photons and is only chirped half as much, its chirped temporal duration does not fully envelop the signal photon. As such, it acts partially like a temporal filter, evidenced by the reduction in the herald bandwidth and statistical correlation of the final joint spectrum. An escort pulse with a significantly broader spectrum than the photon would increase the efficiency of the process. Further efficiency concerns could be addressed with higher power escort pulses and materials with stronger nonlinearities, although phase-matching restrictions must be carefully considered.

By analogy to a light beam incident off center to a lens, introducing a relative delay between the escort pulse and input signal results in a shift in the central wavelength of the joint spectrum, as shown in Fig. 4. This occurs as the relationship between the instantaneous frequencies of the chirped signal and antichirped escort are shifted, resulting in an overall central frequency shift. By tuning the relative

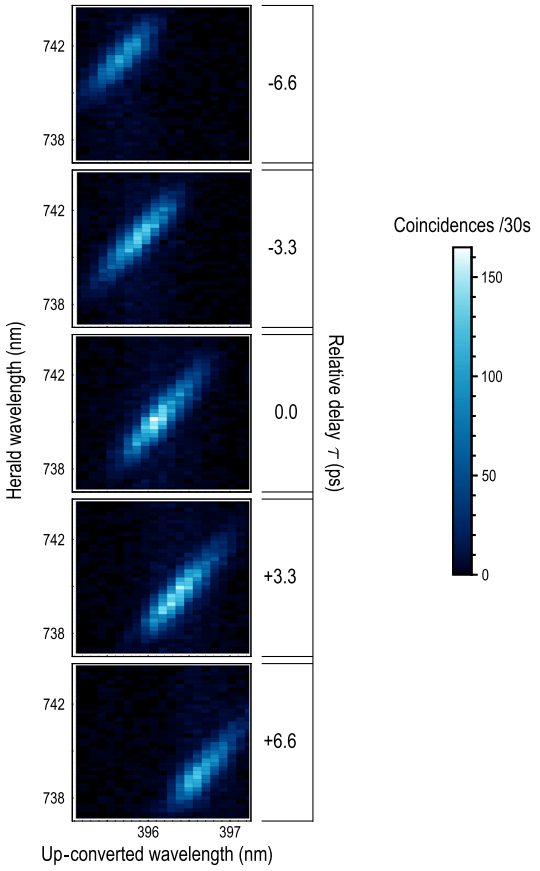


FIG. 4. Tunability of the joint spectra. The center frequency of the joint spectrum is tunable by introducing a relative delay between the input signal and the escort pulse, as seen in the five measured joint spectra. The central wavelength of the up-converted signal changes by 0.071 nm per picosecond of delay. The herald central frequency is also seen to shift due to the escort acting partially as a temporal filter on the signal.

delay over a range of ~13 ps, the central frequency can be tuned over a range of ~2 THz. However, it is seen that the central wavelength of the herald also changes as the delay is changed, as the up-conversion time lens does not uniformly support the entire bandwidth of the input photon. Once again, ensuring that the escort has a broader bandwidth would solve this problem and allow for high-efficiency tunability over a wide spectral range [35]. Restrictive phase matching of the up-conversion medium will also result in a narrowing of the up-converted signal spectra. These effects are detailed in Supplemental Material [38], Sec. III.

We have demonstrated control of a twin-photon joint spectral intensity through the use of an up-conversion time lens on the ultrafast time scale. The technique presented maintains two-photon correlations and introduces minimal background noise at the target wavelengths. The time lens demonstrated here is an essential component of a general quantum temporal imaging system, capable of essential tasks such as bandwidth compression, time-to-frequency conversion, and all-optical transformations on

time-bin-encoded qubits. Control of the correlation of joint spectra as demonstrated here can be used to create spectrally correlated two-photon states at wavelengths where efficient nonlinear materials with extended phase-matching conditions do not exist [6–8,17]. Such a technique may be directly useful for shaping the spectra of entangled pairs for long-distance communications and quantum-enhanced metrology [5] and, more generally, to mold the time-frequency distributions of single photons for experiments both fundamental and practical.

The authors thank J. Lavoie, M. Karpiński, M. D. Mazurek, and K. A. G. Fisher for fruitful discussions and C. Mastromattei for valuable assistance in the laboratory. We are grateful for financial support from the Natural Sciences and Engineering Research Council, the Canada Foundation for Innovation, Industry Canada, Canada Research Chairs, and the Ontario Ministry of Research and Innovation.

*jdonohue@uwaterloo.ca
†kresch@uwaterloo.ca

[1] J. Nunn, L. J. Wright, C. Söller, L. Zhang, I. A. Walmsley, and B. J. Smith, Opt. Express **21**, 15959 (2013).
[2] S. Tanzilli, W. Tittel, M. Halder, O. Alibart, P. Baldi, N. Gisin, and H. Zbinden, Nature (London) **437**, 116 (2005).
[3] B. Brecht, D. V. Reddy, C. Silberhorn, and M. G. Raymer, Phys. Rev. X **5**, 041017 (2015).
[4] J. Franson, Phys. Rev. A **45**, 3126 (1992).
[5] V. Giovannetti, S. Lloyd, and L. Maccone, Nature (London) **412**, 417 (2001).
[6] T. Lutz, P. Kolenderski, and T. Jennewein, Opt. Lett. **39**, 1481 (2014).
[7] O. Kuzucu, F. N. Wong, S. Kurimura, and S. Tovstonog, Phys. Rev. Lett. **101**, 153602 (2008).
[8] A. Eckstein, A. Christ, P. J. Mosley, and C. Silberhorn, Phys. Rev. Lett. **106**, 013603 (2011).
[9] V. Ansari, B. Brecht, G. Harder, and C. Silberhorn, arXiv:1404.7725.
[10] A. Pe'er, B. Dayan, A. A. Friesem, and Y. Silberberg, Phys. Rev. Lett. **94**, 073601 (2005).
[11] B. Albrecht, P. Farrera, X. Fernandez-Gonzalvo, M. Cristiani, and H. de Riedmatten, Nat. Commun. **5**, 3376 (2014).
[12] M. A. Hall, J. B. Altepeter, and P. Kumar, Phys. Rev. Lett. **106**, 053901 (2011).
[13] P. C. Humphreys, B. J. Metcalf, J. B. Spring, M. Moore, X.-M. Jin, M. Barbieri, W. S. Kolthammer, and I. A. Walmsley, Phys. Rev. Lett. **111**, 150501 (2013).
[14] J. M. Donohue, M. Agnew, J. Lavoie, and K. J. Resch, Phys. Rev. Lett. **111**, 153602 (2013).
[15] S. Nowierski, N. N. Oza, P. Kumar, and G. S. Kanter, in *CLEO: QELS_Fundamental Science* (Optical Society of America, Washington, DC, 2015), pp. FTu2A–5.
[16] A. Eckstein, B. Brecht, and C. Silberhorn, Opt. Express **19**, 13770 (2011).
[17] W. P. Grice, A. B. U'Ren, and I. A. Walmsley, Phys. Rev. A **64**, 063815 (2001).
[18] M. Tsang and D. Psaltis, Phys. Rev. A **73**, 013822 (2006).
[19] B. Kolner, IEEE J. Quantum Electron. **30**, 1951 (1994).
[20] I. A. Walmsley and C. Dorrer, Adv. Opt. Photonics **1**, 308 (2009).
[21] R. Jopson, A. Gnauck, and R. Derosier, IEEE Electron Device Lett. **29**, 576 (1993).
[22] S. Watanabe, T. Naito, and T. Chikama, IEEE Photonics Technol. Lett. **5**, 92 (1993).
[23] M. A. Foster, R. Salem, D. F. Geraghty, A. C. Turner-Foster, M. Lipson, and A. L. Gaeta, Nature (London) **456**, 81 (2008).
[24] R. Salem, M. A. Foster, A. C. Turner, D. F. Geraghty, M. Lipson, and A. L. Gaeta, Opt. Lett. **33**, 1047 (2008).
[25] M. A. Foster, R. Salem, Y. Okawachi, A. C. Turner-Foster, M. Lipson, and A. L. Gaeta, Nat. Photonics **3**, 581 (2009).
[26] C. Gu, B. Ilan, and J. E. Sharping, Opt. Lett. **38**, 591 (2013).
[27] N. Matsuda, Sci. Adv. **2**, e1501223 (2016).
[28] K. A. G. Fisher, D. G. England, J.-P. W. MacLean, P. J. Bustard, K. J. Resch, and B. J. Sussman, Nat. Commun. **7**, 11200 (2016).
[29] J. M. Lukens, O. D. Odele, D. E. Leaird, and A. M. Weiner, Opt. Lett. **40**, 5331 (2015).
[30] M. Karpiński, M. Jachura, L. J. Wright, and B. J. Smith, arXiv:1604.02459.
[31] C. V. Bennett, R. P. Scott, and B. H. Kolner, Appl. Phys. Lett. **65**, 2513 (1994).
[32] J. Huang and P. Kumar, Phys. Rev. Lett. **68**, 2153 (1992).
[33] A. P. Vandevender and P. G. Kwiat, J. Mod. Opt. **51**, 1433 (2004).
[34] I. Agha, S. Ates, L. Sapienza, and K. Srinivasan, Opt. Lett. **39**, 5677 (2014).
[35] J. M. Donohue, M. D. Mazurek, and K. J. Resch, Phys. Rev. A **91**, 033809 (2015).
[36] S. Clemmen, A. Farsi, S. Ramelow, and A. L. Gaeta, arXiv:1601.01105.
[37] J. Lavoie, J. M. Donohue, L. G. Wright, A. Fedrizzi, and K. J. Resch, Nat. Photonics **7**, 363 (2013).
[38] See Supplemental Material at http://link.aps.org/supplemental/10.1103/PhysRevLett.117.243602 for a thorough theoretical description and additional experimental details.
[39] P. G. Kwiat, A. M. Steinberg, and R. Y. Chiao, Phys. Rev. A **47**, R2472 (1993).
[40] J. D. Franson, Phys. Rev. Lett. **62**, 2205 (1989).